



# Beneficial effects of antisymmetric nonlinear damping with application to energy harvesting and vibration isolation under general inputs

Yun-Peng Zhu · Z. Q. Lang

Received: 4 September 2021 / Accepted: 5 April 2022 / Published online: 28 April 2022  
© The Author(s) 2022

**Abstract** Beneficial effects of nonlinear damping on energy harvesting and vibration isolation under harmonic inputs have been investigated showing that the introduction of nonlinear damping can increase the harvested energy and reduce the vibration over both the resonant and higher frequency ranges. However, the scenario becomes more complicated when the loading inputs are of more general form such as multi-tone and random inputs, which can produce system responses that are induced by an interaction of system input components of different frequencies. In the present study, by introducing the concept of power transmissibility, the study of the beneficial effects of nonlinear damping is extended to the systems subject to general inputs including both multi-tone and random inputs. A rigorous analysis is conducted based on single degree of freedom systems subject to general inputs. The analysis reveals the conditions under which the antisymmetric nonlinear damping is beneficial for improving energy harvester performance and reducing of the power of system output in vibration isolation. Moreover, the beneficial effects are demonstrated by two case studies.

**Keywords** Energy harvesting · Vibration isolation · Power transmissibility · Antisymmetric nonlinear damping · Frequency analysis

## 1 Introduction

Additional nonlinear damping has shown many advantages in vibration suppression and exploitation [1–5]. For example, Magneto-rheological (MR) nonlinear damping has been widely applied in vibration isolations for engineering structures such as buildings [1] and vehicles [2]. Recently, nonlinear damping has also been proven to be beneficial for vibrational energy harvesting [3, 5]. These have shown that nonlinear damping can play important roles and have great potential in solving different engineering problems.

The antisymmetric nonlinear damping is a type of damping where the damping force is in proportion to the velocity raised to odd orders [6]. The study of antisymmetric nonlinear damping is a significant area of nonlinear damping-related research as in engineering practice, a large class of damping nonlinearities can be represented by an antisymmetric function of velocity [7]. The exploitation of antisymmetric nonlinear damping for either vibration reduction or energy harvesting has been studied by many researchers [2, 8–12]. For example, it has been shown that the

---

Y.-P. Zhu · Z. Q. Lang (✉)  
Department of Automatic Control and Systems  
Engineering, The University of Sheffield,  
Sheffield S1 3JD, UK  
e-mail: z.lang@sheffield.ac.uk

Y.-P. Zhu  
e-mail: y.y.zhu@sheffield.ac.uk

force transmissibilities of vibration isolation systems are reduced over the resonant frequencies, while unchanged over higher frequencies by an introduction of antisymmetric nonlinear damping [8]. This property has been applied to solve many engineering problems such as building isolation in long period seismic movements [9, 11] and vibration suppression of rotor bearing systems [12]. Co et al. [11] applied a semi-active implementation of the cubic damping-based building isolation systems to achieve better isolation performance for multiple story buildings subject to long period seismic movements. Yan et al. [12] indicate that antisymmetric nonlinear damping suspension can benefit high-speed rotor systems achieving a desired isolation performance with more stable response than the linear damping. Recently, researchers have also explored the application of antisymmetric nonlinear damping in energy harvesting systems [3–5], demonstrating that, under certain conditions, an antisymmetric nonlinear damping-based energy harvester can harvest more energy than a linear energy harvester system. Hendijanizadeh et al. [5] developed an energy harvesting device for small boats and yachts where the dynamic range of the energy harvester was expanded using variable load resistance mechanism that can produce nonlinear damping characters.

However, most current studies on the application of antisymmetric nonlinear damping on vibration isolation and energy harvesting only consider harmonic loadings where system behaviors involve no interactions between input components at different frequencies. Where loading inputs are multi-tone, band-limited or random signals [13, 14], the system dynamics are often more complicated. Some works have been carried out to discuss these problems [13–18] for specific cases. For example, in [13–16], the advantages of applying additional antisymmetric nonlinear damping in vehicle suspension and building isolation systems under random loading conditions had been revealed. However, these advantages were also claimed to be inconspicuous by other studies [17, 18]. Basically, different conclusions can be reached for different application scenarios where specific loading conditions are different. In addition, nonlinear energy harvesters have been studied by considering Gaussian white noise excitations for building base isolation and vehicle suspension systems [19, 20]. It has been shown that an introduction of

nonlinear stiffness can expand the working range of energy harvesters [21]. However, there is still no result showing whether an additional antisymmetric nonlinear damping can achieve a better energy harvesting performance than a linear damping when the energy harvesting system is subject to a general loading input. There is also a lack of rigorous analyses that can reach a definite conclusion about when an antisymmetric nonlinear damping can be beneficial to vibration isolations and energy harvesting when associated systems are subject to loadings more complicated than harmonics.

In the present study, the concept of power transmissibility is introduced to address the difficulties associated with dealing with general loading inputs. The effects of nonlinear damping and the magnitude of loading input on the output power of nonlinearly damped SDOF systems are studied using the output frequency response function (OFRF) [22–24]. The results reveal, for the first time, that with the increase in either antisymmetric nonlinear damping or input magnitude of a nonlinearly damped SDOF system, the power transmissibility decreases if the power of the system input is concentrated over the resonant frequency regions, while unchanged if the power of the system input is located around higher frequencies. These conclusions are significant for the analysis and design of both SDOF nonlinear vibration isolators and SDOF energy harvesters when the system is subject to a general input loading. Two case studies are used to demonstrate the advantages with the application of antisymmetric nonlinear damping to energy harvesting and vibration isolation, respectively.

## 2 Force and power transmissibility of SDOF systems with antisymmetric nonlinear damping

### 2.1 SDOF system with antisymmetric nonlinear damping

The SDOF dynamic systems with an antisymmetric damping are shown in Fig. 1 and can be represented by

$$m\ddot{y}(t) + f_c(t) + ky(t) = u(t) \quad (1)$$

where  $t$  is time;  $u(t)$  represents the force input in Fig. 1a and  $m\ddot{z}(t)$  in Fig. 1b with  $z(t)$  is the displacement of ground movement;  $y(t)$  is the relative displacement output with respect to the ground;  $m$

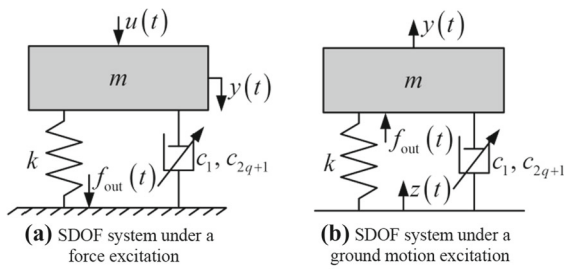


**Fig. 1** SDOF systems with antisymmetric nonlinear damping

and  $k$  are the mass and linear stiffness of the system, respectively;  $f_{out}(t)$  is the force transmitted to the ground in Fig. 1a and represents the force acted on the mass in Fig. 1b; and  $f_c(t)$  is the damping force given by

$$f_c(t) = c_1\dot{y}(t) + \sum_{q=1}^Q c_{2q+1}\dot{y}(t)^{2q+1} \tag{2}$$

with  $c_1$  and  $c_{2q+1}$ ,  $q = 1, \dots, Q$  representing the linear and antisymmetric nonlinear damping coefficients, respectively.

In practice, both linear and antisymmetric nonlinear damping forces can be realized using MR damper [10]- or electromagnetic damper [20]-based active or semi-active control approaches.

The force and power transmissibility of the SDOF system (1) will be introduced in the following.

### 2.2 Force transmissibility

The force transmissibility of a nonlinear system is defined as the ratio between the spectrum of the system force output and the spectrum of the force input [25] given by

$$T_F(\omega) = \left| \frac{F_{out}(j\omega)}{U(j\omega)} \right| \tag{3}$$

where  $\omega$  is the angular frequency, and  $F_{out}(j\omega)$  and  $U(j\omega)$  are the spectra of the force output  $f_{out}(t)$  and the force input  $u(t)$ , respectively.

It has been found that, under single-tone harmonic inputs, an increase in antisymmetric nonlinear damping or input magnitude can reduce the force transmissibility over the resonant frequency range without detrimental effects to the force transmissibility over the non-resonant frequency ranges [3, 25].

For example, for nonlinear system

$$\ddot{y}(t) + c_1\dot{y}(t) + c_3\dot{y}(t)^3 + c_5\dot{y}(t)^5 + 1 \times 10^4 y(t) = u(t) \tag{4}$$

where  $c_1$  is the linear damping coefficient, and  $c_3$  and  $c_5$  are the coefficients of the nonlinear damping, the force output is

$$f_{out}(t) = c_1\dot{y}(t) + c_3\dot{y}(t)^3 + c_5\dot{y}(t)^5 + 1 \times 10^4 y(t) \tag{5}$$

When system (4) is subject to a harmonic input  $u(t) = A \cos(\omega_F t)$  where  $A$  and  $\omega_F$  are the input magnitude and frequency, respectively, the force transmissibility is

$$T_F(\omega_F) = \left| \frac{F_{out}(j\omega_F)}{A} \right| \tag{6}$$

Under different values of the system linear and nonlinear damping coefficients and input magnitudes as given in Table 1, the force transmissibility over the frequency range of  $\omega_F \in [0, 300]$  rad/s is shown in Fig. 2.

Basically, larger force transmissibility means more energy can be harvested [5]. It can be seen in Fig. 2a that under a larger input amplitude of  $A = 5$ , the linear and nonlinear energy harvesting systems have similar force transmissibility around resonance as shown in Cases 2 and 3. But, under a smaller input amplitude of  $A = 1$ , the nonlinear energy harvesting system has a larger force transmissibility than the linear system as shown in Cases 4 and 5. The results, therefore, indicate that overall the nonlinear energy harvester can harvest more energy than the linear one. This conclusion has been reached in [3] and [5]. On the other hand, the results illustrated for Cases 1, 2 and 3 in Fig. 2b clearly demonstrate the significant beneficial effect of nonlinear damping for vibration isolation, which has been revealed in [8, 25].

**Table 1** Different linear and nonlinear damping and input magnitude cases under study

Cases	Parameters
Case 1	$c_1 = 10; c_3 = c_5 = 0; A = 5$
Case 2	$c_1 = 40; c_3 = c_5 = 0; A = 5$
Case 3	$c_1 = 10; c_3 = 2 \times 10^3; c_5 = 2 \times 10^5; A = 5$
Case 4	$c_1 = 40; c_3 = c_5 = 0; A = 1$
Case 5	$c_1 = 10; c_3 = 2 \times 10^3; c_5 = 2 \times 10^5; A = 1$

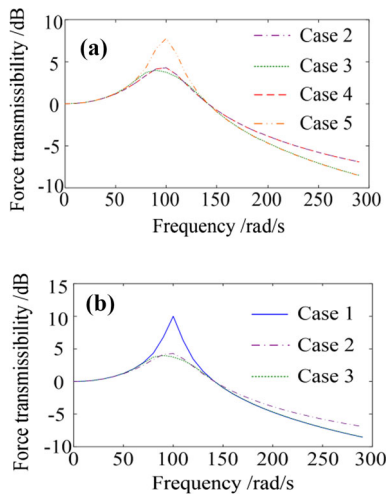


**Fig. 2** The force transmissibilities of different cases

However, when a system is subject to a general loading input such as multiple and random loadings, the above results cannot be directly applied. This is because under general inputs, the system output forces often contain the components covering a range of frequencies which are dependent on the interaction of the input components of different frequencies and, therefore, cannot be separately investigated. But it is expected that if the input loadings only contain components over either the resonant frequency range or the non-resonant frequency ranges, a nonlinear damping should also be beneficial for both vibration isolation system and energy harvesting just as in the case where the system is subject to harmonic loadings.

In order to study and confirm these expectations, the concept of power transmissibility will be first introduced.

### 2.3 The power transmissibility

The energy of signal  $x(t)$  can be represented using the Parseval theorem as [26]

$$\begin{aligned}
 P_x &= \int_{-\infty}^{+\infty} |x(t)|^2 dt = \int_{-\infty}^{+\infty} |X(j\omega)|^2 \frac{d\omega}{2\pi} \\
 &= 2 \int_0^{+\infty} |X(j\omega)|^2 \frac{d\omega}{2\pi}
 \end{aligned} \tag{7}$$

where  $X(j\omega)$  is the spectrum of  $x(t)$ .

In order to study the effects of antisymmetric nonlinear damping under general inputs, the spectra of the input and output signals over three different ranges

of frequencies will be taken into account separately. The three ranges are

$$\begin{aligned}
 I_L &\subseteq \left[ 0, \frac{\sqrt{2}}{2} \omega_r \right); \quad I_R \subseteq \left[ \frac{\sqrt{2}}{2} \omega_r, \sqrt{2} \omega_r \right]; \\
 I_H &\subseteq \left( \sqrt{2} \omega_r, +\infty \right]
 \end{aligned} \tag{8}$$

where  $\omega_r$  is the resonant frequency of the SDOF system under study and  $I_L$ ,  $I_R$  and  $I_H$  represent the low-frequency, resonant frequency and high-frequency ranges, respectively. The high-frequency range  $I_H$  is defined by the isolation range of SDOF systems [4], while the resonant frequency range is defined symmetric to the resonant frequency  $\omega_r$ . In addition, denote

$$\begin{cases}
 P_{u, LH} = 2 \left( \int_0^{\frac{\sqrt{2}\omega_r}{2}} |U(j\omega)|^2 \frac{d\omega}{2\pi} + \int_{\sqrt{2}\omega_r}^{+\infty} |U(j\omega)|^2 \frac{d\omega}{2\pi} \right) \\
 P_{u, R} = 2 \int_{\frac{\sqrt{2}\omega_r}{2}}^{\sqrt{2}\omega_r} |U(j\omega)|^2 \frac{d\omega}{2\pi} \\
 P_{f_{out}, LH} = 2 \left( \int_0^{\frac{\sqrt{2}\omega_r}{2}} |F_{out}(j\omega)|^2 \frac{d\omega}{2\pi} + \int_{\sqrt{2}\omega_r}^{+\infty} |F_{out}(j\omega)|^2 \frac{d\omega}{2\pi} \right) \\
 P_{f_{out}, R} = 2 \int_{\frac{\sqrt{2}\omega_r}{2}}^{\sqrt{2}\omega_r} |F_{out}(j\omega)|^2 \frac{d\omega}{2\pi}
 \end{cases} \tag{9}$$

are input and output power over non-resonant frequencies (subscript ‘‘LH’’) and resonant frequencies (subscript ‘‘R’’), and define the input power ratio

$$\Upsilon_{in} = \frac{P_{u, LH}}{P_{u, R} + P_{u, LH}} \in [0, 1] \tag{10}$$

and the output power ratio

$$\Upsilon_{out} = \frac{P_{f_{out}, LH}}{P_{f_{out}, R} + P_{f_{out}, LH}} \in [0, 1] \tag{11}$$

to represent the percentage of power over non-resonant frequencies in the input and output signal, respectively.

Then, the power transmissibility of system (1) in terms of  $\Upsilon_{in}$  can be defined as

$$T_P(\Upsilon_{in}) = \frac{P_{f_{out}}(\Upsilon_{in})}{P_u(\Upsilon_{in})} = \frac{\int_0^{+\infty} |F_{out}(j\omega)|^2 d\omega}{\int_0^{+\infty} |U(j\omega)|^2 d\omega} \tag{12}$$

where  $P_{f_{out}}(\Upsilon_{in})$  and  $P_u(\Upsilon_{in})$  represent the energy of the system output  $f_{out}(t)$  and input  $u(t)$  in terms of  $\Upsilon_{in}$ , respectively.

In the following, the effect of antisymmetric nonlinear damping on the power transmissibility of

SDOF nonlinear systems subject to general inputs will be analyzed.

### 3 Beneficial effects of antisymmetric nonlinear damping on SDOF systems under general inputs

#### 3.1 The frequency domain representation

The output response of nonlinear systems asymptotically stable around zero equilibrium can be represented by a Volterra series as [27]:

$$y(t) = \sum_{n=1}^N \int_{-\infty}^{+\infty} \cdots \int_{-\infty}^{+\infty} h_n(\tau_1, \dots, \tau_n) \prod_{i=1}^n u(t - \tau_i) d\tau_i \tag{13}$$

where  $N$  is the maximum truncation order of the Volterra series, and  $h_n(\tau_1, \dots, \tau_n)$  is the  $n$ th-order Volterra kernel.

In the frequency domain, the system output spectrum  $Y(j\omega)$  can be represented as [27]

$$Y(j\omega) = \sum_{n=1}^N \frac{1}{\sqrt{n}(2\pi)^{n-1}} \int_{\omega_1+\dots+\omega_n=\omega} H_n(\omega_1, \dots, \omega_n) \times \prod_{i=1}^n U(j\omega_i) d\sigma_\omega \tag{14}$$

where  $\int_{\omega_1+\dots+\omega_n=\omega} [\cdot] d\sigma_\omega$  denotes the integration over the hyperplane  $\omega_1 + \dots + \omega_n = \omega$  with  $d\sigma_\omega$  representing an infinitely small element on the hyperplane,  $\omega_1, \dots, \omega_n$  are the frequency variables, and

$$H_n(\omega_1, \dots, \omega_n) = \int_{-\infty}^{+\infty} \cdots \int_{-\infty}^{+\infty} h_n(\tau_1, \dots, \tau_n) \times \exp[-j(\omega_1\tau_1 + \dots + \omega_n\tau_n)] d\tau_1 \cdots d\tau_n \tag{15}$$

is the  $n$ th-order generalized frequency response function (GFRF) of the system, which can be determined from the system’s differential equation model using a recursive algorithm [28].

From (14), the system output spectrum  $Y(j\omega)$  can be represented by a polynomial function of the system parameters which define the system nonlinearity in the differential equation model of the system, known as the output frequency response function (OFRF) [22].

For nonlinear system (1) with an antisymmetric nonlinear damping, the OFRF representation of the system output spectrum  $F_{out}(j\omega)$  is given in Lemma 1.

**Lemma 1:** *The OFRF representation of the output spectrum of system (1) can be written as.*

$$F_{out}(j\omega) = F_1(j\omega) + \sum_{v=1}^{\lfloor (N-1)/2 \rfloor} F_{2v+1}(j\omega) \tag{16}$$

where  $\lfloor \cdot \rfloor$  denote to take the integer,

$$\begin{cases} F_1(j\omega) = [1 - m\omega^2 L(\omega)]U(j\omega) & v = 0 \\ F_{2v+1}(j\omega) = \sum_{(j_1, \dots, j_Q) \in \mathbf{J}_{(2v+1)}} \Phi_{2v+1}^{(j_1, \dots, j_Q)}(j\omega) & v \geq 1 \\ \times c_3^{j_1} \cdots c_{2Q+1}^{j_Q} & \end{cases} \tag{17}$$

$$\begin{aligned} \Phi_{2v+1}^{(j_1, \dots, j_Q)}(j\omega) &= \frac{m\omega^2}{\sqrt{2v+1}(2\pi)^{2v}} \\ &\times \int_{\omega_1+\dots+\omega_{2v+1}=\omega} L(\omega_1, \dots, \omega_{2v+1}) \\ &\times \prod_{i=1}^{2v+1} L(\omega_i)(-j\omega_i)U(j\omega_i) \\ &\times \left[ \sum_{z=1}^{\bar{v}} \prod_{i=1}^{\bar{z}} \frac{j\omega_{l_i(1)}^{(z)} + \cdots + j\omega_{l_i(j_v)}^{(z)}}{L^{-1}(\omega_{l_i(1)}^{(z)}, \dots, \omega_{l_i(j_v)}^{(z)})} \right] d\sigma_\omega \end{aligned} \tag{18}$$

$$L(\omega_1, \dots, \omega_{2v+1}) = - \left[ \frac{m(j\omega_1 + \cdots + j\omega_{2v+1})^2}{+c(j\omega_1 + \cdots + j\omega_{2v+1}) + k} \right]^{-1} \tag{19}$$

and  $\mathbf{J}_{(2v+1)}$  is a set of  $Q$ -dimensional nonnegative integer vectors containing the exponents of monomials  $c_3^{j_1} \cdots c_{2Q+1}^{j_Q}$ ;  $\bar{v}$  and  $\bar{z}$  in (18) are the integers dependent on  $v$ , and

$$\omega_{l_i(j_v)}^{(z)} \in \{\omega_1, \dots, \omega_{2v+1}\}, j_v = 1, 3, \dots, 2v + 1.$$

**Proof of Lemma 1** See details in [6, 25].

Based on the OFRF representation (16), the power transmissibility of system (1) will be analyzed next.

### 3.2 Effects of antisymmetric nonlinear damping on SDOF system power transmissibility

First, consider the power transmissibility  $T_P(\Upsilon_{in})$  of system (1) with an antisymmetric nonlinear damping in the case of  $\Upsilon_{in} \approx 0$ . Denote the input frequency range of the system as  $\mathbf{W}_{in}$ , and assume the output response over the frequency range produced by higher-order system nonlinearities due to the effect of intermodulation which are negligible [25, 29]. In this case, an important property of the power transmissibility  $T_P(\Upsilon_{in})$  can be summarized in Proposition 1.

**Proposition 1** Consider system (1) subject to input  $u(t) = \alpha \bar{u}(t)$  where  $\alpha > 0$  and  $\bar{u}(t)$  is a given baseline input. If  $\Upsilon_{in} \approx 0$ , then (i)  $\mathbf{W}_{in} \subseteq \pm I_R$ , (ii)  $\Upsilon_{out} \approx 0$ , and (iii) there exists a  $\bar{c}_{2q+1} > 0$ ,  $q = 1, \dots, Q$  such that when  $0 < c_{2q+1} < \bar{c}_{2q+1}$ ,

$$\frac{\partial T_P(\Upsilon_{in})}{\partial c_{2q+1}} < 0 \text{ and } \frac{\partial T_P(\Upsilon_{in})}{\partial \alpha} < 0 \tag{20}$$

**Proof of Proposition 1** See Appendix A.

Proposition 1 shows that if the input of system (1) only contains energy over the resonant frequency range, the power transmissibility of the system decreases when either a coefficient of the antisymmetric nonlinear damping or the magnitude of the system input increases.

On the other hand, consider the power transmissibility  $T_P(\Upsilon_{in})$  of system (1) in the case of  $\Upsilon_{in} \approx 1$ , properties can be revealed via studying the boundary of the system power transmissibility in Proposition 2.

**Proposition 2** If  $\Upsilon_{in} \approx 1$ , then (i)  $\mathbf{W}_{in} \subseteq \pm(I_L \cup I_H)$ , (ii)  $\Upsilon_{out} \approx 1$ , and (iii).

$$T_P(\Upsilon_{in}) \leq \bar{T}_P(\Upsilon_{in}) \approx \frac{\int_{\mathbf{W}_{in}} \bar{F}_1^2 d\omega}{\pi P_u(\Upsilon_{in})} \tag{21}$$

where  $\bar{T}_P(\Upsilon_{in})$  is independent from either the nonlinear damping parameters or the input magnitude  $\alpha$ , and  $\bar{F}_1$  is the boundary of the linear damping force  $F_1(j\omega)$ .

**Proof of Proposition 2** See Appendix B.

Proposition 2 shows that when the input of system (1) only contains energy over the non-resonant frequency range, the power transmissibility of the

system will be bounded by the same boundary on that of the corresponding linear system.

Propositions 1 and 2 imply that when the input of system (1) only contains energy over the system resonant frequency range, the power transmissibility decreases when either the value of the antisymmetric nonlinear damping coefficients or the input magnitude increases. However, when the input contains energy outside the system resonant frequency range, the power transmissibility does not vary with either the nonlinear damping parameters or the amplitude of the input. In the following, an example will be used to illustrate the implication of the conclusions of Propositions 1 and 2.

### 3.3 An example

In the following, system (4) is used as an example to demonstrate the effects of antisymmetric nonlinear damping on the power transmissibility of the SDOF nonlinear systems represented by Eq. (1).

The resonant frequency of system (4) is  $\omega_r = 100$  rad/s, and according to (8), the three frequency ranges of  $I_L$ ,  $I_R$  and  $I_H$  are given by

$$\begin{aligned} I_L &\subseteq [0, 70.7]\text{rad/s}; I_R \subseteq [70.7, 141.4]\text{rad/s}; I_H \\ &\subseteq (141.4, +\infty)\text{rad/s} \end{aligned} \tag{22}$$

Consider a band-limited input

$$u(t) = \alpha \bar{u}(t) \tag{23}$$

where

$$\bar{u}(t) = \frac{A_0 \sin[(\omega_{st} + 70)(t - t_0)] - \sin[\omega_{st}(t - t_0)]}{\pi(t - t_0)} \tag{24}$$

with  $t \in [0, 2t_0]$ ,  $t_0 = 3\text{s}$ ,  $\omega_{st} \in [0, 210]$  rad/s,  $A_0 = 0.5$  N and  $[\omega_{st}, \omega_{st} + 70]$  being the frequency range of the band-limited input.

The total power of  $\bar{u}(t)$  is

$$\begin{aligned} P_u &= \int_{\mathbf{W}_{in}} \bar{U}(j\omega)^2 d\omega = (\omega_{st} + 70 - \omega_{st})A_0^2 \\ &= 17.5 \text{ W} \end{aligned} \tag{25}$$

and  $\bar{u}(t)$  under different  $\omega_{st} \in [0, 210]$  rad/s is shown in Fig. 3.

The power ratio  $\Upsilon_{in}$  of  $\bar{u}(t)$  is obviously a function of  $\omega_{st}$ , which can be obtained as

$$\Upsilon_{in} = \begin{cases} \frac{A_0^2 |\omega_{st} - 70.7|}{P_u} & \omega_{st} \leq 141.4 \text{ rad/s} \\ 1 & \text{Others} \end{cases} \quad (26)$$

Table 2 shows the different values of  $c_1, c_3, c_5$  and  $\alpha$  that are used to evaluate the power transmissibility of system (4) when the system is subject to input (24). The power transmissibility evaluated against the input power ratio  $\Upsilon_{in}$  for the different cases in Table 2 is shown in Fig. 4.

In Fig. 4, the bottom axis is the start frequency  $\omega_{st}$  of the input frequency range, while the top one shows the input power ratio  $\Upsilon_{in}$ .  $\Upsilon_{in}$  starts with  $\Upsilon_{in} = 1$  because  $P_{u,R} = 0$  at the beginning when the input frequency range is within  $I_L$ . Then,  $\Upsilon_{in}$  reduces to  $\Upsilon_{in} = 0$  due to  $P_{u,LH} = 0$  when the input frequency range is within  $I_R$ . Finally,  $\Upsilon_{in}$  gets back to  $\Upsilon_{in} = 1$  as  $P_{u,R} = 0$  again when the input frequency range is within  $I_H$ .

The results in Fig. 4a illustrate what has been revealed in Propositions 1 and 2. For example, by comparing the results in Cases 2, 3, 4 and 5, it can be seen that when  $\Upsilon_{in}$  is around zero and  $\alpha = 1$ , the power transmissibility of the system under linear damping (Case 2) is similar to that under antisymmetric nonlinear damping (Case 3). However, when  $\alpha$  is reduced from 1 to 0.2, the antisymmetric nonlinear damping (Case 5) can produce higher power transmissibility than what can be produced by the linear

**Table 2** Different linear and nonlinear damping parameters and input magnitudes considered in the example

Cases	Parameters
Case 1	$c_1 = 10; c_3 = c_5 = 0; \alpha = 1$
Case 2	$c_1 = 40; c_3 = c_5 = 0; \alpha = 1$
Case 3	$c_1 = 10; c_3 = 2 \times 10^3; c_5 = 2 \times 10^5; \alpha = 1$
Case 4	$c_1 = 40; c_3 = c_5 = 0; \alpha = 0.2$
Case 5	$c_1 = 10; c_3 = 2 \times 10^3; c_5 = 2 \times 10^5; \alpha = 0.2$
Case 6	$c_1 = 40; c_3 = 2 \times 10^3; c_5 = 2 \times 10^5; \alpha = 1$

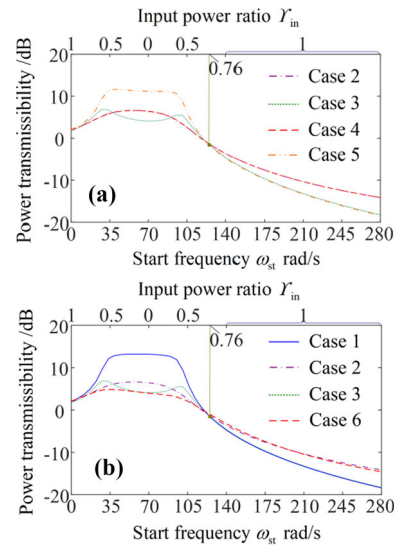


**Fig. 4** The power transmissibility against the range of input frequencies (represented by  $\omega_{st}$ )/power ratio of input  $\Upsilon_{in}$

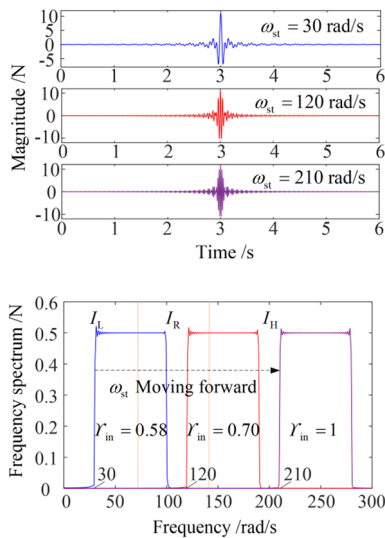


**Fig. 3** The time and frequency domain representation of  $\bar{u}(t)$  under different  $\omega_{st}$

damping (Case 4). This is the conclusion of Proposition 1 and is greatly beneficial to vibrational energy harvesting, which will be demonstrated in Case study 1 in Sect. 4.

In addition, the results of Cases 2 and 3 in Fig. 4b indicate that the power transmissibility under a linear damping (Case 2) and the power transmissibility under an antisymmetric nonlinear damping (Case 3) are similar when  $\Upsilon_{in}$  is around zero. But, when  $\Upsilon_{in} \geq 0.76$ , the antisymmetric nonlinear damping (Case 3) can produce lower power transmissibility than that with the linear damping (Case 2). On the other hand, it can also be observed from Fig. 4b that with the same linear damping  $c_1 = 40$  in Case 2 and Case 6, the antisymmetric nonlinear damping (Case 6) can produce a lower power transmissibility when  $\Upsilon_{in}$  is around zero,

and a similar power transmissibility over  $Y_{in} \geq 0.76$  showing again an overall superior performance of nonlinear damping over linear damping.

These analyses confirm the conclusion of Proposition 2 and can significantly benefit vibration isolation, which will be demonstrated in Case study 2 in Sect. 4.

It is worth emphasizing that, as far as we are aware, this is the first time that these beneficial effects of nonlinear damping have been rigorously revealed for SDOF system (1) for the cases where the system is subject to a general band-limited loading input.

### 4 Case studies

#### 4.1 Case study 1—application to energy harvesting subject to random excitations

Vibrational energy harvesting has attracted great interests in engineering practice, and various structures and devices have been proposed such as the piezoelectric energy harvesting [30] and electromagnetic energy harvesting [31]. It has been shown in [3, 5] that, under harmonic excitations, a cubic damping has better performance than a linear damping in energy harvesting under both higher and lower level excitations. In this case study, the application of cubic damping in an energy harvester subject to random excitations is studied based on the analysis results in Sect. 3.

A vibrational energy harvester as shown in Fig. 5 is used in this study [5], where  $m_1$  is the mass of the harvester,  $k_1$  is the linear stiffness, and  $c_1$  and  $c_{n3}$  are the linear and cubic nonlinear damping coefficients, respectively. A rotational energy storage is applied to absorb vibration energy, which is composed of a ball screw driven by the vibrating mass that drives a generator on top of the energy harvester. The energy

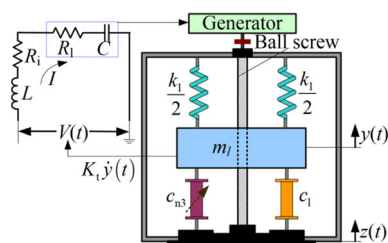


**Fig. 5** The vibrational energy harvester with a nonlinear cubic damping

harvesting circuit is shown in Fig. 5, where  $I$  is the current,  $R_i$  is the resistance related to the energy dissipation and  $R_l$  is the resistance related to the energy absorption, and  $C$  and  $L$  are the inductance and the capacitance of the circuit, respectively. The voltage across the circuit  $V(t) = K_t \dot{y}(t)$  is dependent on the velocity of the mass, where  $K_t$  is the electromagnetic coupling coefficient.

The energy harvester in Fig. 5 can be represented as

$$m\ddot{y}(t) + (c_1 + c_e)\dot{y}(t) + c_{n3}\dot{y}(t)^3 + k_1y(t) = -m\ddot{z}(t) \tag{27}$$

where  $y(t)$  is the relative displacement of the mass and  $z(t)$  is the displacement of the base,  $c_e$  is the equivalent damping coefficient of the energy absorption circuit,  $m = m_1 + m_0$  with  $m_0 = J(2\pi/l_0)^2$  being the inertia of the system,  $J$  is the moment of inertia of the system, and  $l_0$  is the lead size of lead screw [5].

When neglecting the effect of  $C$  and  $L$ , there is [5]

$$c_e = \frac{K_t^2}{R_i + R_l} \tag{28}$$

The absorbed instant power of the vibrational energy harvester in Fig. 5 can then be given as [32]

$$P_{VEH}(t) = \frac{1}{R_l} \left[ \frac{R_l}{R_i + R_l} V(t) \right]^2 = \frac{R_l K_t^2}{(R_i + R_l)^2} \dot{y}(t)^2 \tag{29}$$

and the absorbed energy can be obtained as

$$\begin{aligned} P_{VEH} &= \int_{-\infty}^{+\infty} p_{VEH}(t) dt \\ &= \int_0^{+\infty} \frac{2R_l K_t^2}{(R_i + R_l)^2} |(j\omega)Y(j\omega)|^2 \frac{d\omega}{2\pi} \\ &\approx \sum_{n=0}^{\lfloor N_s/2 \rfloor} \frac{2R_l K_t^2}{(R_i + R_l)^2} \left| \left( j \frac{2\pi n f_s}{N_s} \right) Y \left( j \frac{2\pi n f_s}{N_s} \right) \right|^2 \frac{f_s}{N_s} \end{aligned} \tag{30}$$

where  $f_s$  is the sampling frequency, and  $N_s$  is the number of the total sampling points.

It is worth noting that the test rig of vibrational energy harvester illustrated in Fig. 5 was built with linear damping in [5]. The model (27) and the harvested energy (30) have been experimentally verified [5], based on which beneficial effects of cubic nonlinear damping on vibration energy harvesting can be exploited. In practice, the cubic nonlinear damping



force can be realized using electromagnetic damper or MR damper based on semi-active control approaches developed in [2, 10, 11].

It can be seen from (30) that the absorbed energy is only dependent on the output spectrum  $Y(j\omega)$  when circuit parameters  $R_i, R_1$  and  $K_t$  are fixed. On the other hand, the output force can be written as

$$f_{out}(t) = (c_1 + c_e)\dot{y}(t) + c_{n3}\dot{y}(t)^3 + k_1y(t) = -m\ddot{z}(t) - m\dot{y}(t) \tag{31}$$

and the output power of the vibrational energy harvester is

$$P_{f_{out}}(\Upsilon_{in}) = 2 \int_0^{+\infty} |F_{out}(j\omega)|^2 \frac{d\omega}{2\pi} = 2 \int_0^{+\infty} |m\omega^2[Z(j\omega) + Y(j\omega)]|^2 \frac{d\omega}{2\pi} \tag{32}$$

The power transmissibility of the energy harvester can therefore be obtained as

$$T_P(\Upsilon_{in}) = \frac{P_{f_{out}}(\Upsilon_{in})}{P_u(\Upsilon_{in})} = \frac{\int_0^{+\infty} |\omega^2[Z(j\omega) + Y(j\omega)]|^2 d\omega}{\int_0^{+\infty} |\omega^2 Z(j\omega)|^2 d\omega} \tag{33}$$

It can be seen from (33) that, under an input excitation spectrum  $Z(j\omega)$ , a large power transmissibility  $T_P(\Upsilon_{in})$  indicates a large output displacement  $Y(j\omega)$  over the output frequency range, so as to produce more  $P_{VEH}$  to be absorbed as shown in (30).

Now, consider the case where:

- (a) System (27) is subject to an input with  $\Upsilon_{in} \approx 0$ .
- (b) The input has driven the relative displacement  $y(t)$  to the maximum bound, and
- (c) A linear and a corresponding cubic nonlinear energy harvester are adopted such that the power harvested by system (27) using the linear and nonlinear damping is the same.

Then, according to Proposition 1, it is known that if the magnitude of the inertial force  $-m\ddot{z}(t)$  now decreases by a constant factor, the cubic nonlinear damping-based energy harvester can absorb more energy than the energy that can be absorbed by the linear damping-based energy harvester.

This beneficial effects of nonlinear damping have been demonstrated by researchers when the system is subject to a harmonic input [3, 5]. However, under the

conditions of (a)–(c), the same conclusion can be reached by applying Proposition 1 to system (27) which is subject to a general input. In the following, a specific case of system (27) will be used to demonstrate this significant and more general beneficial effect of nonlinear damping on vibrational energy harvesting.

Take the parameters of the linear vibrational energy harvester in Fig. 5 as [5]

$$m = 8.3 \text{ kg}, k_1 = 250 \text{ N/m}, K_t = 7.57 \text{ N/A}, R_i = 1.3 \Omega, R_1 = 7 \Omega \tag{34}$$

such that the resonant frequency is  $\omega_r = 5.488 \text{ rad/s}$ .

1000 different realizations of two band-limited random inputs are produced by passing Input 1  $\ddot{z}(t) = 10\text{rand}(t)$  and Input 2  $\ddot{z}(t) = \text{rand}(t)$  through a low-pass filter with pass band  $\omega \in (\pi, 3\pi) \text{ rad/s}$ , respectively. The output spectrum  $|Y(j\omega)|$  of system (27) to one realization of Input 1 under a linear damping with  $c_1 = 10.1 \text{ Ns/m}$ ,  $c_{n3} = 0$  and a nonlinear damping with  $c_1 = 0$ ,  $c_{n3} = 2 \times 10^3 \text{ Ns}^3/\text{m}^3$ , respectively, is shown in Fig. 6a.

The absorbed output power is evaluated using (27) to assess the energy harvesting performance of system (27). Over the 1000 different realizations of the band-limited random Input 1 under the linear and nonlinear damping, respectively, the absorbed power results are statistically analyzed and shown in the box plot in Fig. 6b.

On the other hand, the corresponding output spectrum and absorbed power of system (27) to the

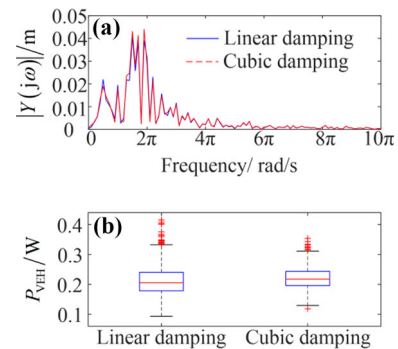


**Fig. 6** The output responses and energy harvesting performance of system (27) subject to input 1 under linear and cubic damping

band-limited random Input 2 are shown in Fig. 7a, b, respectively.

The results in Figs. 6 and 7 demonstrate how an antisymmetric nonlinear damping can benefit energy harvesters when the system is subject to ambient random vibrations as revealed rigorously in Proposition 1. Some detailed explanations are as follows.

In practice, the maximum  $y(t)$  that can be exploited by energy harvester (27) is limited due to space constraint [3, 5]. Figure 6 shows the case where a linear and cubic nonlinear damping-based energy harvester is both subject to Input 1 (a random loading around the system resonance) and achieves a similar performance. Assuming that Input 1 represents the scenario where  $y(t)$  in system (27) reaches the exploitable maximum. Then, according to [3], it is known that the adopted linear and cubic nonlinear damping in this case is equivalent. Therefore, since Input 2 has less amplitude than Input 1 representing a normal (non-extreme) random loading scenario, the results in Fig. 7 demonstrate that the cubic nonlinear damping performs better than its equivalent linear damping for the energy harvester system (27) in normal working conditions and, consequently, has an overall advantage.

The average energy conversion efficiency can be computed as  $\eta = \sum_{i=1}^{1000} P_{VEH,i} / \sum_{i=1}^{1000} P_{c,i}$  [33], where  $P_{VEH,i}$  represents the literally harvested vibration energy under the  $i$ th realization of the random input determined from (30), while

$$\begin{aligned}
 P_{c,i} &= \int_{-\infty}^{+\infty} \left[ (c_1 + c_e) \dot{y}_{(i)}(t) + c_{n3} \dot{y}_{(i)}(t)^3 \right] dt \\
 &\approx \sum_{n=0}^{\lfloor N_s/2 \rfloor} \left[ (c_1 + c_e) \left| \left( j \frac{2\pi n f_s}{N_s} \right) Y_{(i)} \left( j \frac{2\pi n f_s}{N_s} \right) \right| \frac{f_s}{N_s} \right. \\
 &\quad \left. + c_{n3} \left| \left( j \frac{2\pi n f_s}{N_s} \right) Y_{(i)} \left( j \frac{2\pi n f_s}{N_s} \right) \right|^3 \frac{f_s}{N_s} \right] \tag{35}
 \end{aligned}$$

where  $y_{(i)}(t)$  and  $P_{c,i}$  represent the output response and the energy that is absorbed by the damping mechanism of the system under the same random input realization. It can be shown that the average energy conversion efficiency achieved by cubic and linear damping is  $\eta_{non} = 39.08\%$  and  $\eta_{lin} = 34.24\%$ , respectively, under Input 1 and  $\eta_{non} = 84.22\%$  and  $\eta_{lin} = 34.24\%$ , respectively, under Input 2. This indicates a significant advantage of cubic nonlinear damping over linear damping in energy harvesting performance with average energy conversion efficiency increasing from 34.24% to 84.22% in the case of Input 2.

It is worth pointing out that the benefits discussed above are the unique contribution of antisymmetric nonlinear damping to vibrational energy harvesting compared to nonlinear stiffness-based energy harvesters. Nonlinear energy harvesters with hardening nonlinear stiffness may extend the energy harvesting working range under harmonic excitations [34], but this is not the case when the system is subject to random excitations [35]. Energy harvesters based on quasi-zero stiffness are widely applied in practice especially when the system is subject to low-frequency vibrations [36]. An additional antisymmetric damping in this case will further improve the energy harvesting performance under low-frequency vibrations according to the results in this study proposed in Proposition 1.

#### 4.2 Case study 2—Application to vibration isolation of a physical building model subject to seismic waves

Building isolation systems are important for vibration isolation during earthquakes, and low stiffness bearings are usually applied to shift the structural resonant frequencies well below the frequencies of ground motions. However, severe long period earthquakes have been recorded, for example, in the Tohoku

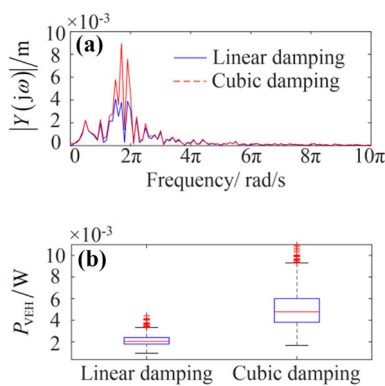


**Fig. 7** The output responses and energy harvesting performance of system (27) subject to input 2 under linear and cubic damping

earthquake in 2011 [37]. In this case, traditional low stiffness-based vibration isolator may not satisfy the required building isolation performance [38]. The issue can be resolved by using the nonlinear damping-based isolator. This has been studied in [11] where both a numerical and a scaled down laboratory model of the Sosokan building in Keio University in Japan has been used to demonstrate the advantage of nonlinear damping over linear damping in building isolation when a building is subject to long-period sinusoidal ground motions.

However, in most earthquakes, the ground motions are random signals. In this case study, the power transmissibility of a nonlinearly damped physical building model subject to seismic waves is experimentally investigated to demonstrate the advantage of nonlinear damping over linear damping in building isolation applications during earthquakes.

A scaled down Sosokan building physical model is shown in Fig. 8, which is a 2-story building system and can be written as

$$\mathbf{M}\ddot{\mathbf{x}} + \mathbf{C}\dot{\mathbf{x}} + \mathbf{K}\mathbf{x} = \mathbf{E}u_{\text{con}} + \mathbf{F}\ddot{z} \tag{41}$$

where  $u_{\text{con}}$  represents the controlled damping force, and

$$\mathbf{x} = \begin{bmatrix} x_1 \\ x_2 \end{bmatrix}; \mathbf{M} = \begin{bmatrix} m_1 & 0 \\ 0 & m_2 \end{bmatrix}; \mathbf{C} = \begin{bmatrix} c_1 + c_2 & -c_2 \\ -c_2 & c_2 \end{bmatrix};$$

$$\mathbf{K} = \begin{bmatrix} k_1 + k_2 & -k_2 \\ -k_2 & k_2 \end{bmatrix}; \mathbf{E} = \begin{bmatrix} 1 \\ 0 \end{bmatrix}; \mathbf{F} = \begin{bmatrix} -m_1 \\ -m_2 \end{bmatrix}$$

with  $x_1, x_2$  being the relative displacement of the first and the second floor to the ground, respectively.

The parameters of the test rig are taken as

$$m_1 = 3.672 \text{ Kg}, m_2 = 1.696 \text{ Kg}, k_1 = 1036 \text{ N/m},$$

$$k_2 = 5868.7 \text{ N/m}, c_1 = 0.0856 \text{ Ns/m},$$

$$c_2 = 0.5367 \text{ Ns/m} \tag{42}$$

where it can be found that the second natural frequency of the test rig (11.5 Hz) is much higher than the first natural frequency (2.0 Hz) due to the low base stiffness  $k_1$ . Considering that the dominant frequencies of seismic waves are much lower than the building's second natural frequency [39], the analysis of the test rig can be conducted based on a SDOF system model.

A nonlinear damping force is generated by using a semi-active damper illustrated in Fig. 9 with three different linear damping coefficients

$$c_{p1} = 4.76 \text{ Ns/m}; c_{p2} = 40 \text{ Ns/m}; c_{p3} = 55.9 \text{ Ns/m} \tag{43}$$

and the shifting time delay of  $T = 0.16 \text{ s}$  [40].

The control of the semi-active damper has been introduced in [11] by using an open-loop control algorithm as

$$c_s(t) = \begin{cases} c_{p1}, & \text{for } u_d/v \leq (c_{p1} + c_{p2})/2 \\ c_{p2}, & \text{for } (c_{p1} + c_{p2})/2 < u_d/v \leq (c_{p2} + c_{p3})/2 \\ c_{p3}, & \text{for } u_d/v > (c_{p2} + c_{p3})/2 \end{cases} \tag{44}$$

as illustrated in Fig. 10 to produce the damping force

$$u_{\text{con}} = -c_s(t)v \tag{45}$$

where  $u_d = -c_{n3}x_1^3$  is the desired nonlinear damping force with  $c_{n3}$  being the desired nonlinear damping coefficient, and  $v = \dot{x}_1$  in this study is the velocity across the damper measured from the first floor of the building.

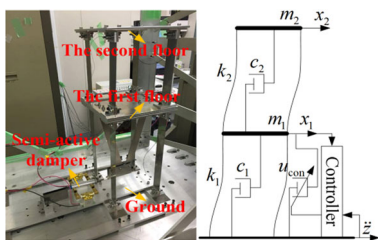


Fig. 8 The scaled down Sosokan building model

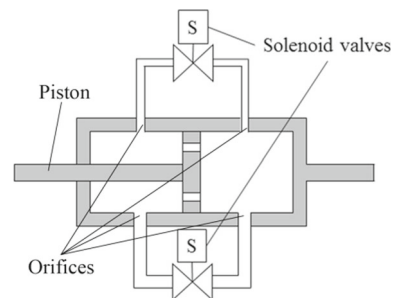
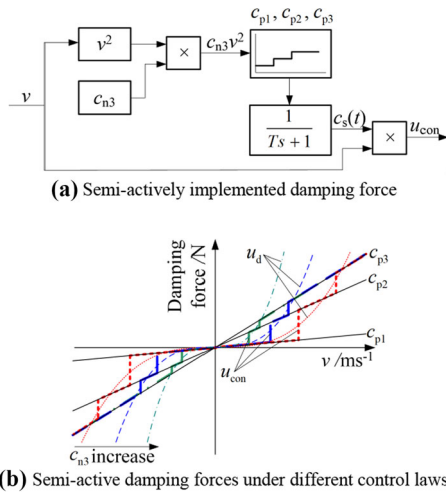


Fig. 9 The structure of the semi-active damper



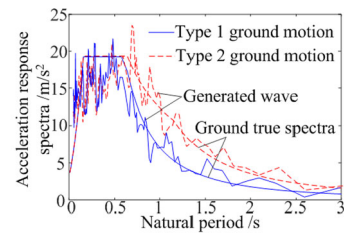
**Fig. 10** The semi-actively implemented nonlinear damping force

Figure 10a shows the semi-active implementation of a nonlinear damping. Figure 10b shows the implemented antisymmetric nonlinear damping. Basically, the implementation approach selects the best linear damping coefficient such that a damping force  $u_{con}$  close to the desired nonlinear damping force  $u_d$  can be produced.

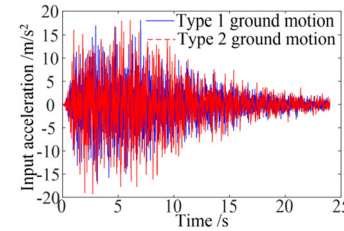
The Kokuji seismic waves, known as the simulated earthquake motions fitted to a target response acceleration spectrum of the Building Standard Law Enforcement Order of Japan [41], are generally used in the design and analysis of building isolation systems [42]. In the experiment, two different Kokuji seismic waves are applied to study the isolation performance of the nonlinear damping-based building isolation system. The two Kokuji seismic waves are generated from the response spectra shown in Fig. 11a, producing two types of ground motions, the hard (Type 1) and soft (Type 2) ground motions as shown in Fig. 11b.

According to Propositions 1 and 2 and the example in Sect. 3.3, it is expected that nonlinear damping could improve the isolation performance when most frequency components that the ground motion contains are in the non-resonant frequency range of the building model.

In the experiment, the power transmissibility from the ground to the first floor of the test rig computed from the absolute accelerations is considered with the sampling frequency of  $f_s = 100$  Hz:



**(a)** The response spectra of ground motions



**(b)** Seismic ground motions generated from the response spectra

**Fig. 11** The response spectra and corresponding time history of seismic ground motions

$$\begin{aligned}
 T_P(\Upsilon_{in}) &= \frac{P_{f_{out}}(\Upsilon_{in})}{P_u(\Upsilon_{in})} = \frac{\int_0^{+\infty} |\omega^2 [Z(j\omega) + X_1(j\omega)]|^2 d\omega}{\int_0^{+\infty} |\omega^2 Z(j\omega)|^2 d\omega} \\
 &\approx \frac{\sum_{n=0}^{\lfloor N_s/2 \rfloor} \left| \left( \frac{2\pi n f_s}{N_s} \right)^2 \left[ Z\left( j \frac{2\pi n f_s}{N_s} \right) + X_1\left( j \frac{2\pi n f_s}{N_s} \right) \right] \right|^2}{\sum_{n=0}^{\lfloor N_s/2 \rfloor} \left| \left( \frac{2\pi n f_s}{N_s} \right)^2 Z\left( j \frac{2\pi n f_s}{N_s} \right) \right|^2} \quad (46)
 \end{aligned}$$

where  $N_s$  is the number of the total sampling points.

The power ratio of Type 1 Kokuji wave is  $\Upsilon_{in,1} \approx 0.86$ , and the ratio for Type 2 Kokuji wave is  $\Upsilon_{in,2} \approx 0.91$ , indicating that Type 2 Kokuji wave has more high-frequency power than Type 1 Kokuji wave. Therefore, when the isolation performance of the building with linear damping and cubic nonlinear damping under Type 1 Kokuji wave is similar, the isolation performance with cubic nonlinear damping is expected to be better than that with linear damping under Type 2 Kokuji wave.

Denote the power transmissibility under the cubic nonlinear isolator as  $T_{P\_non}(\Upsilon_{in})$ , and the power transmissibility under the linear isolator as  $T_{P\_lin}(\Upsilon_{in})$ . In the experiment, the coefficient of the semi-active damper  $c_{p2} = 40$  Ns/m is used as the parameter of the linear isolator, and the corresponding nonlinear damping parameters are tuned to be

$c_{n3} = 6 \times 10^4 \text{ N s}^3/\text{m}^3$ , such that under Type 1 Kokuji wave

$$T_{P\_non}(\Upsilon_{in,1}) \approx T_{P\_lin}(\Upsilon_{in,1}) \approx 1.75 \quad (47)$$

Now, consider the case where the building model is subject to Type 2 Kokuji wave with  $\Upsilon_{in} = \Upsilon_{in,2}$ . In this case, the system's power transmissibility under linear and nonlinear damping is

$$T_{P\_non}(\Upsilon_{in,2}) \approx 1.52 \text{ and } T_{P\_lin}(\Upsilon_{in,2}) \approx 1.56,$$

respectively. The fact

$$T_{P\_non}(\Upsilon_{in,2}) \approx 1.52 < T_{P\_lin}(\Upsilon_{in,2}) \approx 1.56$$

validates the results in Proposition 2 demonstrating a superior performance of nonlinear damping.

It is worth noticing that in the design of building base isolation systems, seismic waves with different response spectra need to be taken into account to evaluate the overall performance of the isolation systems [40, 41]. In this case study, the power transmissibility under both linear and nonlinear damping is about the same under the seismic wave with  $\Upsilon_{in} = \Upsilon_{in,1}$ , which is located around the structural system's resonance frequency. In such scenarios, the overall vibration isolation performance is often considered when loading changes from the motion wave over the range of resonant frequency (such as the case with  $\Upsilon_{in} = \Upsilon_{in,1}$ ) to the motion wave over the range of higher frequencies (such as the case with  $\Upsilon_{in} = \Upsilon_{in,2}$ ) [43, 44]. In this study, the vibration isolation performance is assessed by using the reduction of the power transmissibility when loading changes from  $\Upsilon_{in} = \Upsilon_{in,1}$  to  $\Upsilon_{in} = \Upsilon_{in,2}$  under linear and nonlinear damping isolators by referring  $T_{P\_non}(\Upsilon_{in,1}) \approx T_{P\_lin}(\Upsilon_{in,1}) \approx 1.75$  in (47), which are obtained as

$$\begin{cases} T_{P\_lin}(\Upsilon_{in,1}) - T_{P\_lin}(\Upsilon_{in,2}) = 0.19 \\ T_{P\_non}(\Upsilon_{in,1}) - T_{P\_non}(\Upsilon_{in,2}) = 0.23 \end{cases} \quad (48)$$

respectively. The results indicate that the use of nonlinear damping can achieve an extra  $\eta_r = (0.23 - 0.19)/0.19 = 21.05\%$  reduction of the power transmissibility than the use of linear damping.

## 5 Conclusions

The benefits of antisymmetric nonlinear damping to vibration isolation and energy harvest have been studied when a SDOF system is subject to a harmonic loading. However, when the system is subject to general loadings such as multi-tone and random inputs, no conclusions have yet been reached about these benefits due to the complexities with associated analysis.

In order to address this problem, in this study, the concept of power transmissibility is introduced to study the benefits of antisymmetric nonlinear damping to vibration isolation and energy harvesting for SDOF systems subject to general loadings. The results show, for the first time, that with the increase in either an antisymmetric nonlinear damping coefficient or the input magnitude, the power transmissibility decreases if the power of the loading input is mainly concentrated over the system resonant frequency region, while is unchanged if the input power is mainly located beyond the region of the system resonance. An example and two case studies have been used to demonstrate these beneficial effects of antisymmetric nonlinear damping on vibration isolation and energy harvesting under general inputs. In general, this study reveals a significant principle that can be applied to the development of a wide range of mechatronic systems for more effective vibrational energy harvesting and vibration isolation performances.

**Acknowledgements** This work was supported by the UK EPSRC and Royal Society. The authors would also like to thank Prof. Masayuki Kohiyama for his supporting the experimental tests at Keio University, Japan.

**Funding** Funding was provided by UK EPSRC and Royal Society.

**Availability of data and material** The datasets generated during and/or analyzed during the current study are available from the corresponding author on reasonable request.

**Declarations**

**Conflict of interest** The authors declare that they have no conflict of interest.

**Code availability** Not available.

**Open Access** This article is licensed under a Creative Commons Attribution 4.0 International License, which permits use, sharing, adaptation, distribution and reproduction in any medium or format, as long as you give appropriate credit to the original author(s) and the source, provide a link to the Creative Commons licence, and indicate if changes were made. The images or other third party material in this article are included in the article’s Creative Commons licence, unless indicated otherwise in a credit line to the material. If material is not included in the article’s Creative Commons licence and your intended use is not permitted by statutory regulation or exceeds the permitted use, you will need to obtain permission directly from the copyright holder. To view a copy of this licence, visit <http://creativecommons.org/licenses/by/4.0/>.

**Appendix A**

When  $Y_{out} \approx 0$ , most of the output energies are concentrated in the resonant frequency range and non-resonant frequency energies are neglectable. This means the system is excited by input including most energies in the resonant frequency range, and the input power ratio can be given as  $Y_{in} \approx 0$ , such that  $W_{in} \subseteq \pm I_R$ . Two cases are discussed as follows.

If only the  $q_0$ th nonlinear damping is nonzero, there is

$$c_{2q+1} \begin{cases} \neq 0 & q = q_0 \\ = 0 & q \neq q_0 \end{cases} \tag{49}$$

Considering that the output power is an integration of the squared output force spectrum,  $|F_{out}(j\omega)|^2$  is obtained as

$$\begin{aligned} |F_{out}(j\omega)|^2 &= F_{out}(j\omega)F_{out}(-j\omega) = F_1(j\omega)F_1(-j\omega) \\ &+ m\omega^2 c_{2q_0+1} \begin{bmatrix} F_1(j\omega)\Phi_{2q_0+1}^{(1)}(-j\omega) \\ + F_1(-j\omega)\Phi_{2q_0+1}^{(1)}(j\omega) \end{bmatrix} \\ &+ \sum_{v=2}^{2\lfloor V/2q_0-1 \rfloor} c_{2q_0+1}^v \\ &\times \sum_{q=0}^v m^2 \omega^4 \left[ \Phi_{2q_0q+1}^{(q)}(j\omega)\Phi_{2q_0(v-q)+1}^{(v-q)}(-j\omega) \right] \end{aligned} \tag{50}$$

In Eq. (50), when  $W_{in} \subseteq \pm I_R$ , let  $\omega \approx \omega_r$ , and there is

$$F_1(j\omega) \approx \frac{c - m(j\omega_r)}{c} U(j\omega_r) \tag{51}$$

Noticing  $\omega_1, \dots, \omega_{2q_0+1} \in W_{in}$ , let  $\omega_1, \dots, \omega_{q_0} \approx \omega_r$  and  $\omega_{q_0+1}, \dots, \omega_{2q_0+1} \approx -\omega_r$ , such that  $\omega_1 + \dots + \omega_{2q_0+1} \approx -\omega_r$  and

$$\Phi_{2q_0+1}^{(1)}(-j\omega) \approx \frac{-(j\omega_r)}{\omega_r^2 c_{2q_0+2}} |U(j\omega_r)|^{2q_0} U(-j\omega_r) \tag{52}$$

Therefore, according to (51) and (52), there is

$$\begin{aligned} &F_1(j\omega)\Phi_{2q_0+1}^{(1)}(-j\omega) + F_1(-j\omega)\Phi_{2q_0+1}^{(1)}(j\omega) \\ &\approx \frac{-2m}{c_{2q_0+3}} |U(j\omega_r)|^{2q_0+2} \end{aligned} \tag{53}$$

and substituting (53) into (50), evaluate the partial derivation  $\partial|F_{out}(j\omega)|^2 / \partial c_{2q_0+1}$  as

$$\begin{aligned} \frac{\partial|F_{out}(j\omega)|^2}{\partial c_{2q_0+1}} &\approx -\frac{2m^2 \omega_r^2}{c_{2q_0+3}} |U(j\omega_r)|^{2q_0+2} \\ &+ \sum_{v=0}^{2\lfloor N/2q_0-1 \rfloor} v c_{2q_0+1}^{v-1} \sum_{q=0}^v m^2 \omega_r^4 \\ &\times \left[ \Phi_{2q_0q+1}^{(q)}(j\omega_r)\Phi_{2q_0(v-q)+1}^{(v-q)}(-j\omega_r) \right] \end{aligned} \tag{54}$$

and there must exist a  $\bar{c}_{2q_0+1} > 0$  such that if  $0 < c_{2q_0+1} < \bar{c}_{2q_0+1}$ ,

$$\frac{\partial|F_{out}(j\omega)|^2}{\partial c_{2q_0+1}} < 0 \tag{55}$$

Consequently, according to (55), there is

$$\frac{\partial T_P(Y_{in})}{\partial c_{2q_0+1}} = \frac{1}{\pi P_u(Y_{in})} \int_{W_{in}} \frac{\partial|F_{out}(j\omega)|^2}{\partial c_{2q_0+1}} d\omega < 0. \tag{56}$$

when  $0 < c_{2q_0+1} < \bar{c}_{2q_0+1}$ .

Consider that more than one antisymmetric damping exist in the system with  $c_{2q+1} \neq 0$ ,  $q = 1, \dots, Q$ , the results can be proven by using the same process proposed in [6]. Moreover, when the input is given as  $\alpha u(t)$  with  $\alpha$  being the proportional coefficient of the input magnitude, it can be proven similar as above that

$$\frac{\partial T_P(Y_{in})}{\partial \alpha} = \frac{1}{\pi P_u(Y_{in})} \int_{W_{in}} \frac{\partial|F_{out}(j\omega)|^2}{\partial \alpha} d\omega < 0 \tag{57}$$

Then, Proposition 1 is proven.

**Appendix B**

Based on the output boundary representation of system (1) proposed in [29], the OFRF representation of the bounded output force can be proposed according to Lemma 1 as

$$|F_{out}(j\omega)| \leq \bar{F}_{out} = \bar{F}_1 + \sum_{v=1}^{\lfloor (N-1)/2 \rfloor} \bar{F}_{2v+1} \tag{58}$$

where  $\bar{F}_{out}$  is the boundary,

$$\begin{cases} \bar{F}_1 = \bar{L}_w \left( 1 + m\bar{\Omega}^2 \right) \|u\| & v = 0 \\ \bar{F}_{2v+1} = \frac{\bar{L}_w^{2v+2} m\bar{\Omega}^{2v+3} \|u\|^{2v+1}}{\sqrt{2v+1} (2\pi)^{2v}} \\ \quad \times \sum_{(j_1, \dots, j_Q) \in \mathbf{J}_{(2v+1)}} c_3^{j_1} \dots c_{2Q+1}^{j_Q} \bar{\Theta}_{2v+1}^{(j_1, \dots, j_Q)} & v \geq 1 \end{cases} \tag{59}$$

represents a boundary on the output force contributed by the  $2v + 1$ th-order system nonlinearity with  $v = 0, \dots, \lfloor (V - 1)/2 \rfloor$

$$\begin{cases} \bar{L}_w = \sup_{\omega \in \mathbf{W}_{in}} |L(j\omega)|, \bar{\Omega} = \max\{\omega \in \mathbf{W}_{in}\} \\ \bar{\Theta}_{2v+1}^{(j_1, \dots, j_Q)} = \sum_{z=1}^{\bar{v}} [\bar{L}_w(2v+1)\bar{\Omega}]^z \end{cases} \tag{60}$$

and

$$\|u\| = \max_{\omega \in \mathbf{W}_{in}} \{F^{-1}[|U(j\omega)|], |U(j\omega)|\} \tag{61}$$

where  $F^{-1}[\cdot]$  represents the inverse Fourier transform.

Therefore, a boundary on the power transmissibility can be obtained as

$$\begin{aligned} T_P(\Upsilon_{in}) &\leq \bar{T}_P(\Upsilon_{in}) = \frac{\bar{P}_{f_{out}}(\Upsilon_{in})}{P_u(\Upsilon_{in})} \Big|_{\Upsilon=\Upsilon_p} \\ &= \frac{1}{\pi P_u(\Upsilon_{in})} \int_{\mathbf{W}_{in}} \left( \bar{F}_1 + \sum_{n=1}^{\lfloor (N-1)/2 \rfloor} \bar{F}_{2n+1} \right)^2 d\omega \end{aligned} \tag{62}$$

where  $\bar{T}_P(\Upsilon_{in})$  is this boundary.

When  $\Upsilon_{out} \approx 1$ , most of the output energies are concentrated in the low- and high-frequency range and the resonant frequency energies are neglectable. This means the system is excited by input including most energies in the non-resonant frequency range, and the

input power ratio can be given as  $\Upsilon_{in} \approx 1$ , such that  $\mathbf{W}_{in} \subseteq \pm(I_L \cup I_H)$ . Two cases are discussed as follows.

(a) When  $\mathbf{W}_{in} \subseteq \pm I_L$ , let  $\bar{\Omega}$ ,  $\omega \ll \omega_r$  such that

$$\begin{aligned} \bar{L}_w &= \sup_{\omega \in \mathbf{W}_{in}} |L(j\omega)| = \sup_{\omega \in \mathbf{W}_{in}} \left| m \left[ \omega^2 - \frac{c}{m}(j\omega) - \frac{k}{m} \right] \right|^{-1} \\ &= \sup_{\omega \in \mathbf{W}_{in}} \left| k \left[ \frac{\omega^2}{\omega_r^2} - \frac{c}{m} \left( j \frac{\omega}{\omega_r} \right) - 1 \right] \right|^{-1} \approx \frac{1}{k} \end{aligned} \tag{63}$$

and the boundary of the higher-order output force can be written as

$$\begin{aligned} \bar{F}_{2v+1} &\approx \left( \frac{\bar{\Omega}}{\omega_r} \right)^{2v+2} \frac{\bar{\Omega} \|u\|^{2v+1}}{m^{2v+1} \sqrt{2v+1} (2\pi)^{2v}} \\ &\quad \times \sum_{(j_1, \dots, j_Q) \in \mathbf{J}_{(2v+1)}} c_3^{j_1} \dots c_{2Q+1}^{j_Q} \bar{\Theta}_{2v+1}^{(j_1, \dots, j_Q)} \approx 0 \end{aligned} \tag{64}$$

(b) When  $\mathbf{W}_{in} \subseteq \pm I_H$ , let  $\bar{\Omega}$ ,  $\omega \gg \omega_r$  such that

$$\bar{L}_w = \sup_{\omega \in \mathbf{W}_{in}} \left| k \left[ \frac{\omega^2}{\omega_r^2} - \frac{c}{m} \left( j \frac{\omega}{\omega_r} \right) - 1 \right] \right|^{-1} \approx \frac{1}{m\omega^2} \tag{65}$$

and the higher-order output force bound can be written as

$$\begin{aligned} \bar{F}_{2v+1} &\approx \frac{1}{\omega^{2v+1}} \left( \frac{\bar{\Omega}}{\omega_r} \right)^{2v+3} \frac{\|u\|^{2v+1}}{m^{2v+1} \sqrt{2v+1} (2\pi)^{2v}} \\ &\quad \times \sum_{(j_1, \dots, j_Q) \in \mathbf{J}_{(2v+1)}} c_3^{j_1} \dots c_{2Q+1}^{j_Q} \bar{\Theta}_{2v+1}^{(j_1, \dots, j_Q)} \approx 0 \end{aligned} \tag{66}$$

Consequently, the output power boundary is obtained as

$$\bar{P}_{f_{out}}(\Upsilon_{in}) = \frac{1}{\pi} \int_{\mathbf{W}_{in}} \bar{F}_1^2 d\omega \tag{67}$$

When the input is given by  $\alpha u(t)$ , the boundary of the power transmissibility of the nonlinear system is obtained as

$$\bar{T}_P(\Upsilon_{in}) \approx \frac{\int_{\mathbf{W}_{in}} \alpha^2 \bar{F}_1^2 d\omega}{\pi \alpha^2 P_u(\Upsilon_{in})} = \frac{1}{\pi P_u(\Upsilon_{in})} \int_{\mathbf{W}_{in}} \bar{F}_1^2 d\omega \tag{68}$$

Then, Proposition 2 is proven.

## References

1. Cetin, S., Zergeroglu, E., Sivrioglu, S., Yuksek, I.: A new semiactive nonlinear adaptive controller for structures using MR damper: design and experimental validation. *Nonlinear Dyn.* **66**, 731–743 (2011)
2. Yildiz, A.S., Sivrioglu, S., Zergeroglu, E., Cetin, S.: Nonlinear adaptive control of semi-active MR damper suspension with uncertainties in model parameters. *Nonlinear Dyn.* **79**, 2753–2766 (2015)
3. Tehrani, M.G., Elliott, S.J.: Extending the dynamic range of an energy harvester using nonlinear damping. *J. Sound Vib.* **333**, 623–629 (2014)
4. Dutta, S., Chakraborty, G.: Performance analysis of nonlinear vibration isolator with magneto-rheological damper. *J. Sound Vib.* **333**, 5097–5114 (2014)
5. Hendijanizadeh, M., Elliott, S.J., Ghandchi-Tehrani, M.: Extending the dynamic range of an energy harvester with a variable load resistance. *J. Intell. Mater. Syst. Struct.* **28**, 2996–3005 (2017)
6. Peng, Z.K., Lang, Z.Q., Jing, X.J., Billings, S.A., Tomlinson, G.R., Guo, L.Z.: The transmissibility of vibration isolators with a nonlinear antisymmetric damping characteristic. *J. Vib. Acoust. Trans. ASME* **132**, 014501 (2010)
7. Tang, B., Brennan, M.J.: A comparison of two nonlinear damping mechanisms in a vibration isolator. *J. Sound Vib.* **332**, 510–520 (2013)
8. Peng, Z.K., Lang, Z.Q., Zhao, L., Billings, S.A., Tomlinson, G.R., Guo, P.F.: The force transmissibility of MDOF structures with a non-linear viscous damping device. *Int. J. Non-Linear Mech.* **46**, 1305–1314 (2011)
9. Lang, Z.Q., Guo, P.F., Takewaki, I.: Output frequency response function based design of additional nonlinear viscous dampers for vibration control of multi-degree-of-freedom systems. *J. Sound Vib.* **332**, 4461–4481 (2013)
10. Laalej, H., Lang, Z.Q., Daley, S., Zazas, I., Billings, S.A., Tomlinson, G.R.: Application of non-linear damping to vibration isolation: an experimental study. *Nonlinear Dyn.* **69**, 409–421 (2012)
11. Ho, C., Zhu, Y.P., Lang, Z.Q., Billings, S.A., Kohiyama, M., Wakayama, S.: Nonlinear damping based semi-active building isolation system. *J. Sound Vib.* **1**, 302–317 (2018)
12. Yan, S., Dowell, E.H., Lin, B.: Effects of nonlinear damping suspension on non-periodic motions of a flexible rotor in journal bearings. *Nonlinear Dyn.* **78**, 1435–1450 (2014)
13. Bian, J., Jing, X.: Superior nonlinear passive damping characteristics of the bio-inspired limb-like or X-shaped structure. *Mech. Syst. Signal Proc.* **125**, 21–51 (2019)
14. Hayashi, K., Fujita, K., Tsuji, M., Takewaki, I.: A simple response evaluation method for base-isolation building-connection hybrid structural system under long-period and long-duration ground motion. *Front. Built Environ.* **1**, 2 (2018)
15. Pazoiki, A., Goodarzi, A., Khajepour, A., Soltani, A., Porlier, C.: A novel approach for the design and analysis of nonlinear dampers for automotive suspensions. *J. Vib. Control* **24**, 3132–3147 (2018)
16. Zhu, Y.P., Lang, Z.Q., Kawanishi, Y., Kohiyama, M.: Semi-actively implemented non-linear damping for building isolation under seismic loadings. *Front. Built Environ.* **6**, 1–8 (2020)
17. Elmadany, M.M., El-Tamimi, A.: On a subclass of nonlinear passive and semi-active damping for vibration isolation. *Comput. Struct.* **36**, 921–931 (1990)
18. Lu, Z., Wang, Z., Zhou, Y., Lu, X.: Nonlinear dissipative devices in structural vibration control: a review. *J. Sound Vib.* **423**, 18–49 (2018)
19. Constantinou, M.C., Tadjbakhsh, I.G.: Hysteretic dampers in base isolation: random approach. *J. Struct. Eng.* **111**, 705–721 (1985)
20. Mofidian, S.M., Bardaweel, H.: A dual-purpose vibration isolator energy harvester: experiment and model. *Mech. Syst. Signal Proc.* **118**, 360–376 (2019)
21. Drezet, C., Kacem, N., Bouhaddi, N.: Design of a nonlinear energy harvester based on high static low dynamic stiffness for low frequency random vibrations. *Actuator A-Phys.* **283**, 54–64 (2018)
22. Lang, Z.Q., Billings, S.A., Yue, R., Li, J.: Output frequency response function of nonlinear Volterra systems. *Automatica* **43**, 805–816 (2017)
23. Peng, Z.K., Lang, Z.Q.: The effects of nonlinearity on the output frequency response of a passive engine mount. *J. Sound Vib.* **318**, 313–328 (2008)
24. Guo, P.F., Lang, Z.Q., Peng, Z.K.: Analysis and design of the force and displacement transmissibility of nonlinear viscous damper based vibration isolation systems. *Nonlinear Dyn.* **67**, 2671–2687 (2012)
25. Lang, Z.Q., Jing, X.J., Billings, S.A., Tomlinson, G.R., Peng, Z.K.: Theoretical study of the effects of nonlinear viscous damping on vibration isolation of SDOF systems. *J. Sound Vib.* **323**, 352–365 (2009)
26. Mao, B.Y., Xie, S.L., Xu, M.L., Zhang, X.N., Zhang, G.H.: Simulated and experimental studies on identification of impact load with the transient statistical energy analysis method. *Mech. Syst. Signal Proc.* **46**, 307–324 (2014)
27. Lang, Z.Q., Billings, S.A.: Output frequency characteristics of nonlinear systems. *Int. J. Control* **64**, 1049–1067 (1996)
28. Jing, X.J., Lang, Z.Q., Billings, S.A.: Frequency-dependent magnitude bounds of the generalized frequency response functions for NARX model. *Eur. J. Control* **15**, 68–83 (2009)
29. Zhu, Y.P., Lang, Z.Q.: A new convergence analysis for the Volterra series representation of nonlinear systems. *Automatica* **1**, 108599 (2020)
30. Erturk, A., Inman, D.J.: *Piezoelectric Energy Harvesting*. Wiley, Hoboken (2011)
31. Li, Z., Zuo, L., Luhrs, G., Lin, L., Qin, Y.X.: Electromagnetic energy-harvesting shock absorbers: design, modeling, and road tests. *IEEE Trans. Veh. Technol.* **62**, 1065–1074 (2012)
32. Soliman, M.S.M., Abdel-Rahman, E.M., El-Saadany, E.F., Mansour, R.R.: A wideband vibration-based energy harvester. *J. Micromech. Microeng.* **18**, 115021 (2008)
33. Hendijanizadeh, M., Sharkh, S.M., Elliott, S.J., Moshrefi-Torbati, M.: Output power and efficiency of electromagnetic energy harvesting systems with constrained range of motion. *Smart Mater. Struct.* **22**, 125009 (2013)
34. Diala, U., Mofidian, S.M., Lang, Z.Q., Bardaweel, H.: Analysis and optimal design of a vibration isolation system



- combined with electromagnetic energy harvester. *J. Intell. Mater. Syst. Struct.* **30**, 2382–2395 (2019)
35. Daqaq, M.F.: Response of uni-modal duffing-type harvesters to random forced excitations. *J. Sound Vib.* **329**, 3621–3631 (2010)
  36. Yang, W., Towfighian, S.: Low frequency energy harvesting with a variable potential function under random vibration. *Smart Mater. Struct.* **27**, 114004 (2018)
  37. Kasai, K., Mita, A., Kitamura, H., Matsuda, K., Morgan, T.A., Taylor, A.W.: Performance of seismic protection technologies during the 2011 Tohoku-Oki earthquake. *Earthq. Spectra* **29**, 265–293 (2013)
  38. Dan, M., Masashi, O., Fumito, N., Masayuki, K., Lang, Z.Q.: Experimental study of the effectiveness of semi-actively implemented power-law damping on suppressing the seismic response of a base-isolated building. In: *EACS 2016–6th European Conference on Structural Control*, 2016. Sheffield
  39. Makris, N., Chang, S.P.: Effect of viscous, viscoplastic and friction damping on the response of seismic isolated structures. *Earthq. Eng. Struct. Dyn.* **29**, 85–107 (2000)
  40. Nakamichi, F.: Control of Semi-Active Oil Damper Using Local Sensor for Reducing Equipment Response. Keio University, Keio (2018)
  41. The Building Center of Japan: The Building Standard Law of Japan on CD-ROM August 2011. The Building Center of Japan, Tokyo (2011)
  42. Shirai, K., Kikuchi, M., Ito, T., Ishii, K.: Earthquake response analysis of the historic reinforced concrete temple Otaniha Hakodate Betsuin after Seismic retrofitting with friction dampers. *Int. J. Archit. Herit.* **1**, 1–11 (2018)
  43. Chopra, A.K., Chintanapakdee, C.: Comparing response of SDF systems to near-fault and far-fault earthquake motions in the context of spectral regions. *Earthq. Eng. Struct. Dyn.* **30**, 1769–1789 (2001)
  44. Safari, S., Tarinejad, R.: Parametric study of stochastic seismic responses of base-isolated liquid storage tanks under near-fault and far-fault ground motions. *J. Vib. Control* **24**, 5747–5764 (2018)

**Publisher's Note** Springer Nature remains neutral with regard to jurisdictional claims in published maps and institutional affiliations.